3DPD: A PHOTOGRAMMETRIC PIPELINE FOR PUSH FRAME STEREO CAMERAS

E.Simioni [a, *], C.Re [a], T. Mudric [b], G.Cremonese [a], S.Tulyakov[c], A. Pommerol[d] , N. Thomas[d]

[a] INAF-Astronomical Observatory Padova, Padova, Italy (emanuele.simioni@inaf.it)
[b] University of Rijeka, Faculty of Civil Engineering
[c]Ecole Polytechnique Federale de Lausanne, 1015, Lausanne, Switzerland
[d] Physikalisches Institut,University of Bern, Sidlerstr. 5, 3012 Bern, Switzerland

KEY WORDS: Image Processing, Satellite Images, Software, Digital Photogrammetry

ABSTRACT:

An innovative photogrammetric pipeline has been developed by INAF-Padova for the processing of the stereo images from the CaSSIS (Colour and Stereo Imaging System). CaSSIS is the multispectral stereo push frame camera on board ExoMars TGO (Trace Gas Orbiter) which will image 1.5% of the Mars surface in stereo mode with a spatial resolution of 4.6 m/pixel – the highest resolution single pass stereo capability currently operating at Mars. Data acquisition started in April 2018. The camera is able to provide two images of the same target from two different points of view along the same orbit and within one minute. After the acquisition of the first image, the telescope, with a boresight oriented to 10° with respect to nadir direction, is rotated by 180° and the second image is acquired. The stereo pairs can then be processed to provide the 3D topography of specific targets.
The suite of photogrammetry and imaging tools, named 3DPD (3 Dimensional reconstruction of Planetary Data) (Simioni et al. 2017), is designed for processing stereo push frame data and producing the three-dimensional data for geomorphological analysis of planetary surfaces.
The workflow involves a MATLAB tool for the preparation of the inputs (the mosaicked images and the projection matrices) to be ingested into the 3DPD matching core software. The pipeline is in continuous development and routinely ingests the large numbers of images that CaSSIS is producing at the present time and will continue to acquire in the future.

INTRODUCTION

The aim of this article is to introduce the 3D reconstruction software for planetary surfaces developed by the research group of the Astronomical Observatory of Padova (OAPD-INAF). The group is involved in different imaging systems on board space missions, such as BepiColombo, ExoMars 2016 and JUICE, that are acquiring, or will acquire, stereo pairs of planetary surfaces.
BepiColombo has been launched on 20 October 2018 towards planet Mercury. The Spectrometers and Imagers for the Mercury Planetary Orbiter (MPO) BepiColombo Integrated Observatory SYStem (SIMBIO-SYS) (Cremonese 2019), on board the spacecraft, is equipped with a stereo imaging channel (STC) [1] designed to obtain a global coverage of the planet surface in stereo mode.
The ExoMars Trace Gas Orbiter (EM-TGO) mission, which has been launched on 16 March 2016, is equipped with the stereo camera CaSSIS (Colour and Stereo Imaging System), [2] which has provided 1605 stereo-pairs with different acquisition strategies and different filters modes until MTP16 (Medium Term Planning corresponding to 1 month of operation – July 2019).
The JUICE mission, which will be launched in 2022 with the camera JANUS on board will acquire stereo pairs of the surfaces of the icy satellites of Jupiter, primarily Ganymede.
The INAF-OAPD institute, as part of the CaSSIS team, has the responsibility for generating and archiving the Digital Terrain Models (DTMs). The DTMs archiving group [3] implemented a Repository Dynamic Interface for the management of the requests of DTMs reconstruction and the delivery of the stereo products [4].
STC and CaSSIS use the same type of detector and are both based on the push-frame stereo acquisition mode. The photogrammetric procedures applied for the topographic reconstruction of the planetary surfaces in three dimensions are the same and most of the efforts devoted to the design and integration of the processes will be shared.

In the first Section, an introduction describing the instrumental context is proposed. Section 2 describes the developed software, the structure and all the implemented methods. Section 3 is dedicated to the user interface while the details of the base pipeline are illustrated in Section 4.

* Corresponding author. This is useful to know for communication with the appropriate person in cases with more than one author.

1. CONTEXT

Stereo photogrammetry is a digital image processing technique that allows to metrically extract information about the target observed; providing important support for geomorphological analysis and for the quantitative investigation of the features examined by the camera. Combining a variety of techniques, such as camera calibration, image matching and bundle adjustment, photogrammetry is able to derive 3D information from a pair or a set of overlapping images (Wu, 2017).
The result of this process is the generation of Digital Terrain Models (DTM). Nowadays, the acquisition and stereo-analysis of planetary bodies images is (and will continue to be) one of the most important objectives for many planetary missions.

1.1. Possible applications for the 3DPD software: the stereo cameras for planetary exploration

Image acquisition has experienced great developments in the past two decades, as is evident from an unprecedented wealth of imaging sensors on associated platforms. Most of the stereo systems for acquisitions of planetary surfaces adopt the push-broom approach. The stereo camera for Chang E1 [4] and Mars Express HRSC [6] are examples of this strategy. Both instruments acquire three-line arrays in backward, nadir and forward directions respectively. Each channel array is then mapped in a unique ortho image and it provides, from the same orbit, stereo images for DTM reconstruction. Kaguya TC [7] adopts the same approach but with only two lines, increasing, furthermore, the bit depth from 8 to 10.

Several other instruments, based on the push-broom technique, have provided DTMs even if not specifically designed for providing stereo products. Push-broom cameras such as the Lunar Reconnaissance Orbiter Camera (LROC) [8] of Lunar Reconnaissance Orbiter (LRO) and CTX [9] and HiRISE [12] on board Mars Reconnaissance Orbiter (MRO) take advantage of images acquired from different orbits. The images of the OSIRIS [13] camera on board the Rosetta mission, for the investigation of the 67/P CG comet, have been used to perform the reconstruction of the comet shape exploiting multiple frame images with significant overlapping.

The use of 2D images, which are buffered when the spacecraft moves, guarantees to avoid alignment problems implementing a robust geometry configuration.

The CaSSIS camera for ExoMars-TGO is an example of stereo camera using a single telescope (inclined of + - 10° with respect to the nadir) with a rotational mechanism that allows image acquisition from two different directions.

STC/SIMBIO-SYS also applies a push frame approach adopting two different optical sub-channels [10] focusing on a single detector [11] and it represents a novel instrument concept with strong compactness and high innovation. The same configuration, although with a simpler optical design, will be adopted by the Luna-Resurs-1 orbiter mission [14].

.

INSTRUMENT	Mission	Target	Pixel og [m]	Swath [km]	Focal length [mm]	Stereo Chs	Angle vs Nadir [°]
HRSC	Mars Express	Mars	10	52.2	175	3	0 , ±18.9°
CTX	MRO	Mars	6	30	350	1	D.O.
HiRiSe	MRO	Mars	0.3	6	12000	1	D.O.
TC	Kaguja	Moon	20	19.3	65	2	±15°
Stereo Camera	Chang E1	Moon	120	60	23.3	3	0° , ±16.7°
LROC-NAC	LRO	Moon	0.5	5	700	1	D.O
LROC-WAC		Moon	100	60	6	7	D.O.
STC		Mercury	58	52	95.2	2	±20°
CaSSIS	ExoMars2016	Moon	4.6	9,4	880	1	±10°
Luna-Resurs-1	LR1	Moon	2.5-3	14	125	2	±12.5

Table 1 : The list of the main push-broom (upper part) and push frame (bottom part) cameras with stereo acquisition capabilities and their main parameters including focal length, pixel on-ground resolution, swath, number of channels used for stereo reconstruction, different angles with respect to nadir direction where acquisition are performed in different directions from the same orbit or using Different Orbit (D.O.).

2. 3DPD PIPELINE

Figure 1 shows the block diagram of the photogrammetric pipeline.
It consists of several steps:

i) the creation of the complete orthoimages starting from the framelets (single shot acquisitions),
ii) the computation of the integer disparity map (which define the parallax between the images),
iii) the disparity refinement at the sub-pixel level,

iv) the triangulation phase.

All these steps will be described in details in the following sections.

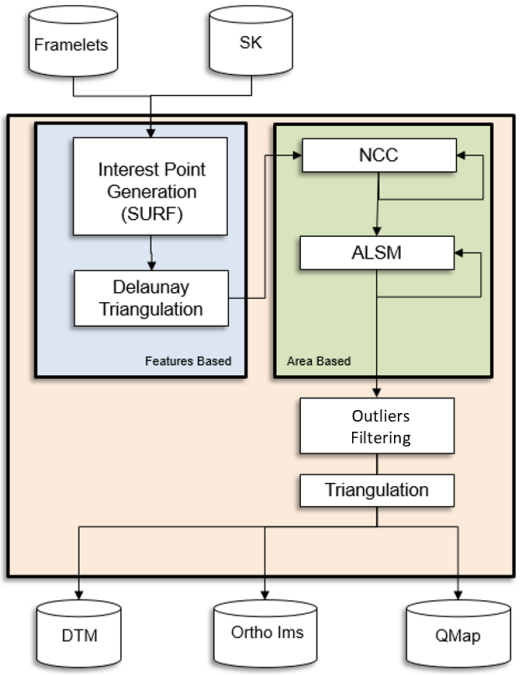

Figure 1 *Block diagram of the processing chain from the Framelets and Spice kernels (SK) to the products.*

2.1. Matching Phase

The first approximation of the disparity map is computed from a large and sparse net of matching points on the stereo couple.
A SURF (Speeded Up Robust Feature) [18] approach is applied to tiles of the original image in a manner that guarantees uniformity of the net on the image. The SURF method, useful in a broad range of applications in computer vision, is a scale and rotation invariant detector (based on the Hessian matrix measure) and descriptor (distribution based). The result of the application of this process is a list of the interest points on both images of the stereo pair. By comparing the descriptors, the pairs of matching points can be found.
The matching points are used for finding sparse disparity, which is then extrapolated to the whole image using Delaunay triangulation and used as initialisation for the Normalized Cross Correlation (NCC) process [20] (see 2.1.2).
A multiresolution approach (image pyramids) is implemented and the NCC is performed on each level of the image pyramid. This process uses a coarse-to-fine approach to reduce the search area and to limit blunders (Corvi and Nicchiotti, 1995).
At the last level of the pyramid (higher resolution) a sub-pixel refinement by area based matching (Least-Squares Matching) is applied (Gruen, 1985) [21].

Three libraries have been developed to manage the main steps of the DTM generation pipeline: i) Interpolation Library ii) NCC Library iii) ALSM Library.

2.1.1. Interpolation Library

The Interpolation library has been developed as “support” to the matching algorithms for the definition of a dense and precise disparity map:

i) The initialization of the parallax map based on SURF[45] tie points.
ii) The interpolation (neighbour or Gaussian-based) of all the image variables considered.
iii) The extrapolation (based on deformable models[22] in case of outliers) of minimal or large regions of the variables.

The first interpolation is used for finding an initial dense disparity map, that is then used for the initialization of NCC. It applies a Delaunay triangulation to the SURF tie points.
The triangulation procedure generates a TIN (Triangulated Irregular Network). The TIN is equivalent to the nerves of the cells in a Voronoi diagram avoiding irregular topologies. For each point of the net it is possible to associate vertical and horizontal disparities which can be interpolated on a grid in order to have a disparity value for each position on the reference image.

The second kind of interpolation (ii) is applied to the images and to the disparity maps during the pyramidal approach to move from higher to lower scale of the images. This kind of interpolation is also used in the tool interface to allow the user to check and to set the data parameters such as gradient component or local standard deviation to be applied to image, quality map or the same disparity map. The last kind of interpolation is used when the user intends to limit the presence of the blunders or artefacts by imposing a manual threshold to the quality map. The deformable models [22] are then applied to fill the resulting holes in the disparity image.

2.1.2. NCC library

The NCC library is based on the implementation of the Normalized Cross Correlation (NCC) similarity function. Normalized cross-correlation has found application in a broad range of computer vision tasks such as stereo vision, motion tracking, image mosaicing, etc.
The main goal of the matching process is to define, in the image space, two physically matching patches (T_1, T_2) in the two images. In time-critical applications, the Sum of Squared Difference (SSD) is often used for the matching patch:

$$S(T_1, T_2) = \sum \left(T_1\big(i + d_i, j + d_j\big) - T_2(i,j) \right)^2 = \sum \delta T^2$$

However, this similarity function has some intrinsic limits: despite the fact that the sampling problem could be solved by a bilinear (or better bi-cubic [24]) interpolation, this similarity function is not invariant to common detector issues such as gain and offset between images. In the literature, this problem has been addressed by introducing a composite function ρ:

$$S(T_1, T_2) = \sum \rho(\delta T)$$

This is the case of the Sum of Absolute Differences (SAD), which represents the Geman McClure Function, or the MAD (Median of Absolute Distance). Although fast and reducing the problem, these similarity functions were replaced by the NCC (Normalized Cross Correlation) invariant to mean (and so to bias) and to scalar values (and so to gain).

$$S(T_1, T_2) = \sum \frac{\left(T_1\left(i+d_i, j+d_j\right) - \overline{T_1}\right)\left(T_2(i,j) - \overline{T_2}\right)}{\sigma_1 \sigma_2} \quad (1$$

Where $\overline{T_i}$,are the means of the templates and σ_i their standard deviation.
This definition allows comparing regions with different intensity without being biased by their values.
In 3DPD, the NCC is optimized by using tables (running sum) containing the integral of the image and of its square [25]. The same idea (not implemented in our workflow but noteworthy) suggests the use of the summing tables for a stronger fast approximation of the NCC in [27].
The Normalized Cross Correlation is the simplest but effective method as a similarity measure, which is invariant to linear brightness and contrast variations. The image matching methods based on Normalized Cross-Correlation cannot perform well when there are strong perspective variations between the images or the Euclidean ones such as significant rotation and scale changes. This is due to the limitation that normalized cross-correlation is sensitive to rotation and scale changes.
As defined in (1) the NCC is limited to pixel grid which will generate discrete parallax maps. In 3DPD a bi-dimensional parabolic interpolation [30] is used to compute sub pixel disparity map but it shows the phenomenon known as *pixel-locking* [28], which produces artificially peaked histograms of sub-pixel disparity.

Considering that most of the Instruments defined in *Table 1* have a non-zero emission angle and often acquire stereo observations from different orbits, the stereo images should be "warped" to each other by the software to obtain similar geometry.

2.1.3. ALSM Library

The ALSM [20] employs an iterative geometric and radiometric transformation between a reference image and a search image in order to minimize the least-squares sum of pixel value differences (SSD) between the images. The method has been named "adaptive" because it can be executed in a self-tuning mode, meaning that the parameter set to be estimated can be corrected automatically in order to obtain the most appropriate estimation of the model set-up with respect to the specific signal content of the patches to be matched. To keep the overall model simple but still effective in most implementations the radiometric parameters permit a linear contrast stretch while the geometric parameters permit an affine transformation. The 6-parameters affine model is an approximation of the actual transformation between the two images. It works generally well when the object surface in the search area is planar, patches are small and images are not too different.
The six parameters are estimated by least-square adjustments using the pixel values from the template as observations. Given two corresponding image patches $T_1(x,y)$ and $T_2(x,y)$, accounting for image noise $N(x,y)$ and for a linear radiometric transformation (concerning the contrast and brightness correction) with parameters *r0, r1* we can write:

$$T_1(x,y) = r_0 + r_1 T_2(u_{x,y}, v_{x,y}) + \mathrm{N}(x,y) \quad (2$$

where

$$\begin{cases} u_{x,y} = a_0 + a_1 x + a_2 y \\ v_{x,y} = b_0 + b_1 x + b_2 y \end{cases} \quad (3$$

is the affine transformation that locally links the homologous pixels between the patch and the template.
The convergence radius of LSM is relatively small (a few pixels):a good approximation of the disparity map is therefore necessary [35] to initialize the process.
Both translation parameters a0 and b0 are of major importance as they define the relative shift between reference and search image as well as the coordinates of the corresponding points. Linearization of (2) with respect to the parameters (a0, ..., b2) requires the computation of the derivatives of the pixel values with respect to (u,v) using numerical approximations.

The adjustment equations must be solved iteratively. At every iteration, the unknowns are corrected. This leads to new pixel value differences between search and reference images, until the sum of squared differences of the corrections is less than a predefined threshold or a specific number of iterations is reached.
The ALSM_Library allows:

- to define the template dimensions,
- to define the maximum number of iterations,
- to repeat the process with different template sizes or pyramid levels

The quality of the ALSM results is limited by the following: illumination and reflectance properties (lack of image texture, shadows, specular reflections), image quality (low signal-to-noise ratio, image artefacts), panoramic problems (due to excessive emission angles), or incorrect initialization of the starting disparity map.
In all these cases a statistical semi-automatic detection of the outliers allows us to discard the outliers and fill the resulting holes with disparity extrapolated from neighborhood regions.

3. TECHNICAL DESCRIPTION AND ARCHITECTURE OF THE SOFTWARE

The software is developed in C SHARP language and it takes advantage of preprocessing tools developed in MATLAB.
The code is multithreaded and works on the Windows Operating System (Windows 7 SP 1 or later, 64 bit).

Language	C#, Matlab
SO	Windows 7 SP 1 or later (64 bit),
Recommended Configuration	Intel Core i7 multi processor 16 GB of RAM
Inputs	8-16 bit stereo images
Products	See Table 2.

Table 1 Main software characteristics

The input framelets/images can be accepted in EDR (Engineering Data Records) format and/or in other more common image formats (JPG, TIFF, PNG) or even as Matlab binary file. Camera parameters and geometry information (i.e. intrinsic and extrinsic parameters) can be included as text files or read directly from Spice Kernels [17]. The generated DTM can be exported in raster format (GeoTIFF) with the corresponding orthoimage; also point clouds and meshes textured (or not) can be provided.
The architecture of the data storage is matrix based (map): the disparity and quality maps are defined as float jarred arrays. This approach has been chosen to guarantee an efficient exploitation for all the intermediate products in the pipeline and to make the user interactions easier during the procedures (such as filtering or quality control).

The main products of the 3DPD pipeline are generated to permit scientific and engineering analysis of the three-dimensional reconstructions. The outputs of the software package include orthoimages (either in radiance factor or raw signal in DN –digital numbers) and additional images products for a better exploitation and understanding of the stereo products, such as a texturized height map and the "Figure of Merit" for the definition of the quality of the matching for each pixel of the gridded DTM. The main 3DPD products are listed in **Table 2**.

Prefix	Description
DTM	a GEOTiff file (extension: TIF or ASC) defined by a matrix with maximum size 2048x8400 of double/float. The DTMs are provided with a nominal spatial resolution of 3 pixels or 1 pixel when a user needs it for a particular analysis. The output pipeline even supports 3D formats such as OGJ or WRL.
HMP	Each DTM is delivered with an RGB image representing the DTM as the height map in hue and the image in intensity.
OTH	Full resolution orthoimages (always in TIF, JP2 and ASC format) for the panchromatic images (in radiance factor) used for the reconstruction.
QMP	Figure of Merit for the fidelity of the reconstruction. Its legend is reported in the XML file.
XML	Text file containing all the Tags of the DTM (as close as possible to PDS 4 standards).

Table 2 *Main 3DPD products and their description.*

4. GUI (GRAPHICAL USER INTERFACE)

Even though the software has been designed to be as much automatic as possible, a user-friendly interactive processing is possible through the software's Graphical User Interface (GUI). The interactive approach offers more control over specific and critical steps of the photogrammetric process.
Through the GUI it is possible to choose different steps of the workflow which have to be executed as well as to define related parameters, such as window template dimension, search area dimension, number of pyramidal levels, similarity functions, outlier thresholds, ALSM iterations number.

The GUI Interface can also provide some statistical and visual representation of all the intermediate data products as matrix structures: the images, the corresponding statistical parameters (local standard deviation, local contrast, or gradients), the disparity maps as well as the quality maps (described by the similarity function).

These statistical methods allow the user to have, at any step of the workflow, a global vision of the state of the reconstruction and to intervene in the process when necessary. For example, this allows limiting and avoiding the propagation of the outliers by detecting spikes and cleaning them on the basis of the surrounding disparity shape.
One example of visualization and analysis performed through the GUI is shown in Figure 2.

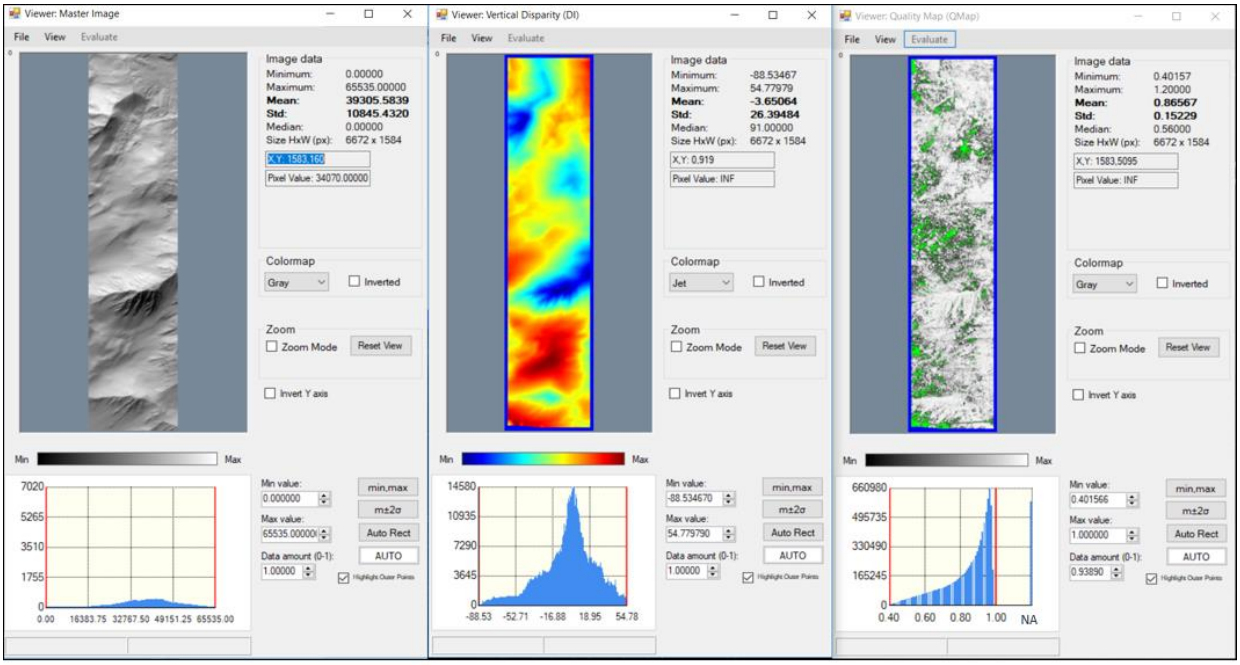

(a)	(b)	(c)

Figure 2 Modular diagram of the software structure. The CaSSIS image shown covers the north-western flank of Olympus Mons, the largest (600 km wide) and tallest (25 km) shield volcano on Mars. Such volcanoes formed during the Hesperian period, and are located between the Tharsis and the Amazonis quadrangle, off the northwestern edge of the Tharsis bulge. The DTM is located over the volcano's outer edge where an escarpment/cliff about 8 km tall is present. The (a) subplot shows the mosaiced image, in (b) the vertical disparity map, in (c) the quality map.

The figure shows: on the left, the master image of the considered stereo couple, in the middle the evaluation of the vertical disparity map, and on the right the quality map.
Each window contains:

-the image considered,
-the main statistical values at first order
-a histogram of the visualized data.

In the case of the Quality map (in this case based on the ALSM) the green pixels show areas where ALSM has not reached convergence.

Since the correlation process can encounter some difficulties, the final results can be affected by a number of mismatches and blunders. The GUI helps to detect the outliers in three different ways:
-by setting a threshold on the quality map;
-by setting the statistical bounds on the disparity maps and on its gradient;
-by setting a threshold on the distance from the local mean (to avoid spike effect);

As shown in Figure 2, these user-defined methods allow, at each stage of the pipeline, to define the regions of failed matching and preserve the continuity on the surface.

At the end of the process, all available information can be saved in jpg format.
As shown in Figure 3: besides the DTM (triangulation of the disparity map shown in Figure 2) the 3DPD provides the texturized height map (in jet color map) of the surface considered and the Figure of Merit which associates to each pixel its fidelity by representing as linear color scales the NCC of the affine based matching in output of the ALSM. In the areas where the 3D reconstruction does not reach convergence (because of saturation, shadow, occlusions, extreme slopes), the red color is used to indicate that the surface is approximated by deformable models.

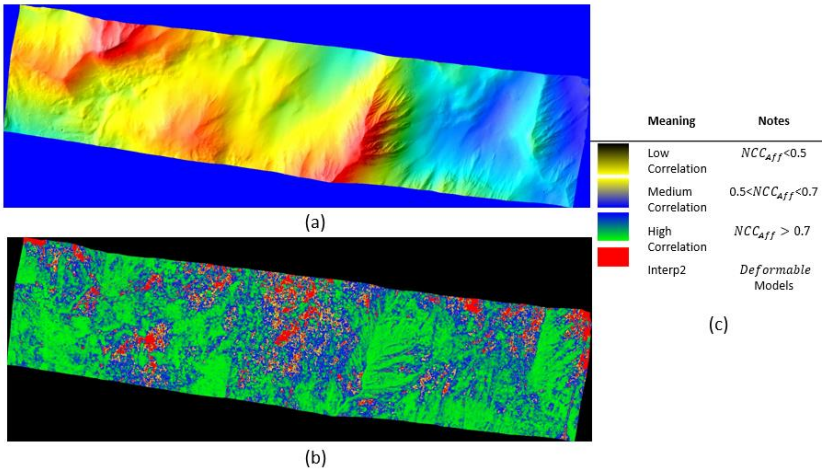

Figure 3 Example of the products of the 3DPD for the case of the CaSSIS images considered in Figure 2. The images represent the height map texturized (a), the Figure of Merit (b) and its legend (c).

5. VALIDATION AND PERFORMANCES

At the base of the validation procedure is the estimation of the performances and of the vertical precision by collecting statistics on the differences between the stereo DTM and a "ground truth" (another topographic data of higher accuracy that can be used as reference) [44], in the following tests:

(i) HERSCHEL_CRATER: based on a pair of synthetic images generated by using the HiRISE Texturized DTM.
(ii) CASSIS_IMAGES: status of the 3D reconstruction with the CaSSIS images
(iii) STC_SVS: based on a couple of images acquired during SIMBIO-SYS STC stereo on-ground validation .
(iv) SLOPE ANGLE TEST: test with synthetic images to analyse the dependence of the vertical precision on the local slope.

5.1. Validation with synthetic images: Herschel Crater

The first test of the 3DPD pipeline was performed shortly after the orbital insertion of TGO on an initial capture orbit in October 19, 2016 and before the beginning of the aerobraking phase.
TGO, at that time, was not on its nominal orbit and the orientations provided by the Spice Kernels were just predicted.
CaSSIS was at a mean distance of 422 km (nominal orbit at 400 km) from the planet surface with a scale difference of 11% between the two acquisitions and a maximal scale of 5.2 m/px.
To test the performance, some synthetic images have been generated starting from a DTM used as reference. The DTM has been produced by the University of Arizona (UA) with the Socet Set SW (©BAE Systems) [20] from stereo pairs by HiRISE [12]. The synthetic images have been created with Blender [23], which is a free and open source 3D creation suite supporting raytracing. Blender allows us to define cameras in the scene, overlay objects with texture and control illumination. Two virtual cameras that simulate the CaSSIS stereo acquisitions have produced images applying a rendering to the artificial scene reproducing the nominal acquisition block geometry of the telescope. The image dimensions are 500x2048 pixels.
For the sake of simplicity, no optical distortion was applied to the images. On the other side, the images are rendered at 10 times the required resolution, introducing an artificial PSF of 1.25 pixels convolved with the images which are then sampled to final resolution. White noise of 10 DN has been added to the images to simulate Read Out Noise (RON).
The reference DTM was imported in Blender and the synthetic images are shown in Figure 4.

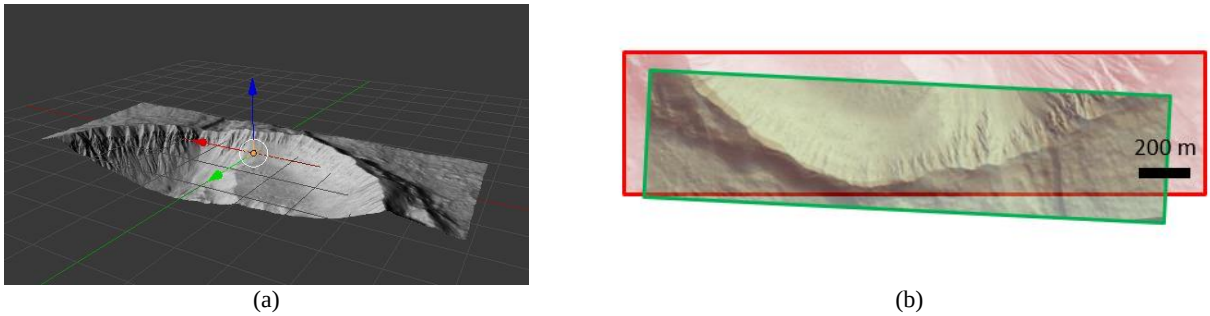

Figure 4 HiRiSe DTM of the Herschel Crater Overlapped images of the Hershel Crater Test.

Using such synthetic images with the orientation parameters defined in Blender, a point cloud has been generated by a dense image matching and the final triangulation; the reconstruction error in the object space was evaluated point-wise as the distance of each point to the reference DTM.
The reference DTM (UA-HiRISE) has been fixed and the DTM reconstruction has been aligned through a 3D modelling software. A threshold of 30 metres, has been considered in order to reject the outliers from the comparison.

Comparison results are shown in **Table 3**.

Data	**Hershel Crater**
Reference	HiRISE DTM.
Pixel on-ground	5.2m
Threshold	30m
# Completeness	91%
Mean	0.03m
RMS	1.1m

Table 3 Reconstruction performance of the SW in HERSCHEL_CRATER test.

The acquisition block geometry introduces a vertical precision of 14.9 metres (considering a parallax error of 1 px) and the software reaches a matching error of 0.1 px, as expected for synthetic images [35].

5.2. Validation with actual CaSSIS Images

Shortly after its arrival at Mars in October 2016, CaSSIS had already demonstrated its stereo performance despite being on a non-nominal orbit. Indeed, the first CaSSIS DTM of a Deep Seated Gravitational Slope Deformation (DSGSD) was reconstructed [32] and analysed [33]. At the end of April 2018, TGO started its commissioning phase and after one Mars year of nominal mission (extended to end of December 2020) it is currently preparing to enter its first mission extension.
Until MTP (Medium Term Planning) 11, CaSSIS had acquired 1492 stereo pairs with different acquisition strategies and with different filter modes. The OAPD team is leading the management of the DTMs requests for science analysis as well as producing them for the scientific community. The management of the request process is performed thanks to the Repository web page [34].
The image processing consists of two main steps. Firstly, a radiometric calibration of the raw data (bias substraction, flatfield division, bad pixels interpolation, straylight and offsets correction) is performed and then the photogrammetric process for the derivation of mosaicked and orthorectified images. The first step is automatically performed by the team at the University of Bern [36]. The latter is systematically performed by the OAPD pipeline every time an MTP is concluded. The process includes the removal of the distortion of the instrument and the generation of ortho-rectified images. Different surfaces are then considered as possible choices: the mean plane on the MOLA surface [39], the Mars spheroid defined in Spice Kernels or the MOLA (463 m/px) body shape.
The mosaicking process is the starting point for the computation of a geometrically consistent solution: the process takes advantage of both the image content and the features. The images allow to minimize “photo plane error” by fixing the geometry of the acquisitions. The features, on the other side, define the stereo block geometry. Their scope is to reach an auto consistent collinearity solution using a non-linear bundle adjustment process.
Different tests were performed to evaluate the performance of the pipeline, in particular in [40] two tests were executed.
In the first test, the matching accuracy of 3DPD has been checked against the one of the ASP (Ames Stereo Pipeline) and with respect to a reference DTM produced by the University of Arizona with Socet Set (SS) with HiRISE [12] stereo images; as also tested in [45]. Since the comparison of the image matching procedure is the objective of the first test, all other steps of the DTM generation procedure have been made independent of the matching software by using the same framework for mosaicking and triangulation developed by EPFL (the code and Ubuntu executable are available online [38]).
In the second test, the performance evaluation of the 3DPD pipeline has been evaluated considering the HiRISE DTMs as data reference (ground truth). The comparisons have demonstrated a relative vertical precision of the 3DPD pipeline of ~5 m [40], comparable to the products of the ASP.
For now, 142 DTMs have been produced with 3DPD. They cover different Mars quadrangles and different purposes.
Figure 5 shows, for example, the DTM produced on the Oxia Planum, a set of 9 DTMs (which represent all the coverage of the region by CaSSIS so far) required by ESA for engineering in order to analyse the landing site of the next ExoMars 2022 mission [37].
.

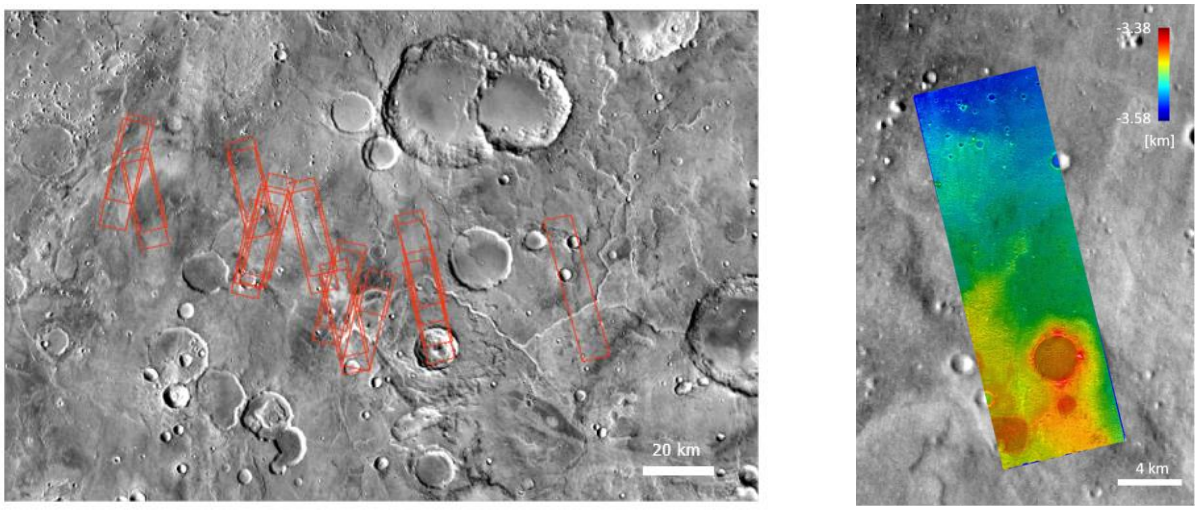

(a) (b)

Figure 5 *(a) shows the footprints of the stereo couples acquired on the Oxia Planum region projected on the Themis global mapping. In (b) showsthe Height Map of the MY34_004172_162 stereo images acquired by CaSSIS at 2018-10-30T13:01:34.410*

The first scientific work making use of a CaSSIS DTM considers the stratigraphic analysis performed on linear profiles of a SPLD (South Polar Layered Deposits). The method, described in [26] considers the extraction of the profile from the DTMs, searching for periodicities in the profiles using wavelet analysis, analysis through Dynamic Time Warping (DTW), a signal-matching algorithm previously used to compare profiles of real and simulated stratigraphy in the NPLD (North Polar Layered Deposits).

Another second example of a Digital Elevation Model (DTM) of an inverted fluvial channel located in Aeolis Planum (4.8878S, 154.8377E) Figure 6. Within the imaged swath, we identified an inverted paleoriverbed with a height of 35 m, a mean Full Width at Half-Maximum (FWHM) of 63 m and a total length of 13km. This structure is of particular importance because it lies close to the ancient coastline of the putative ancient ocean that covered Mars northern plains at the Noachian, possibly being one of its tributaries. This feature is currently being analysed in order to understand the timing of its formation, duration as well as exhumation.

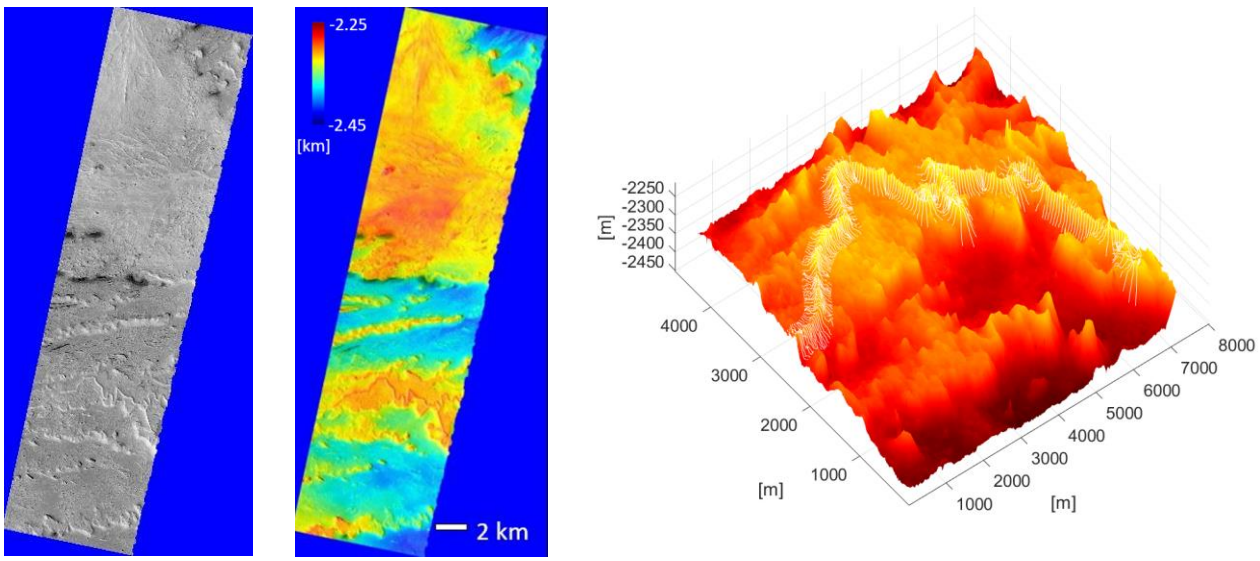

(a) (b) (c)

Figure 6 *The image shows the case of an inverted river around* Aeolis Planum. *This is MY34_004756_354_1 image acquired by CaSSIS at 2018-12-17T09:07:23.158. In (a) we show the orthoimages, in (b) the height map showing in the lower part the inverted river, in (c) zoom of the DTM with the indication of the cross-section of the features.*

5.3. STC-SVS, images for stereo validation

STC [1] is the stereo camera on board the ESA-JAXA BepiColombo mission, that was launched in 2018 toward planet Mercury. STC and CaSSIS are both aiming at surface reconstruction and color imaging, but they use different designs and concepts. STC is, in fact, characterized by two optical channels [41] both inclined of 20° with respect to the nadir direction looking in forward and backward directions. Both channels share a common telescope unit and the detector, a SiPin CMOS (same adopted by CaSSIS) which guarantees a fill factor of 100% thanks to a Back-Side Illumination (BSI) configuration; a focal length of 95.2 mm brought the telescope

performance to achieve an on-ground pixel of 58m (at 480 km from the surface in the first orbit). To test the capabilities of the photogrammetric chain we take advantage of the on-ground STC images: during the calibration campaign of the telescope, in fact, a Stereo Validation Setup (SVS) [42] has been conceived and realized in laboratory in order to validate the new push frame concept of STC [43].
Sets of images have been acquired in the ambient conditions of the clean room with the flight model of STC by means of a collimator lens and two motorized rotators which have reproduced the stereo block geometry of STC operations. The images acquired with the SVS have been used as a test for the pipeline of the SW. In order to evaluate the accuracy of the 3D products, a high resolution laser scanning DTM has been used as reference.

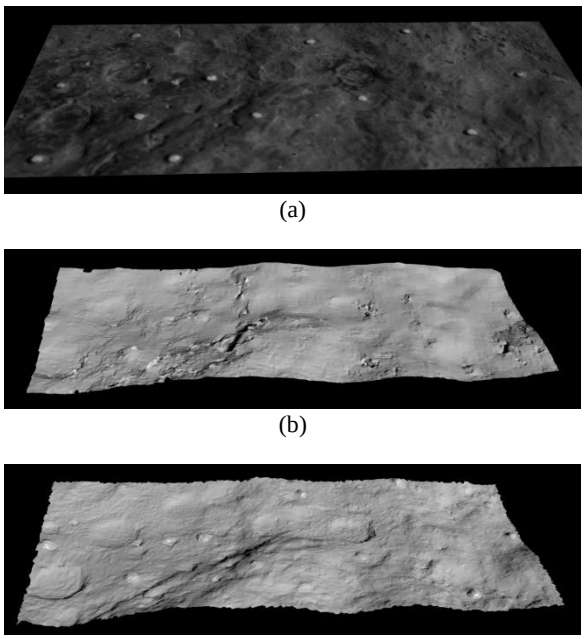

(a) (b) (c)

Figure 7 In the top panel (a) we show the Image obtained by one STC channel of a stone target. In the middle panel (b) the DTM, generated by the pipeline is shown and in the bottom panel (c) the DTM generated by the Laser scanner (ground truth).

The performance of the SW to provide an accurate 3D reconstruction of surfaces has been evaluated using the STC stereo pairs bench also as test. A reference DTM of the rock samples has been provided by a CAM2® Faro Arm Platinum scanner system with a Z axis accuracy of 0.02 mm. The high-resolution laser scanner reconstruction of the sample target has a better vertical accuracy than the one provided by the stereo image reconstruction and has therefore been used as "ground truth" data. The comparison between the stereo DTM and the reference one gave the confidence about the capability of the system.
As a quantitative measure of performance we use the percentile of accepted matches and the Root Mean Square Error (RMSE). RMSE is computed as RMS of the absolute distance of each point from the reference surface.

Data	**STC DTM**
Reference	Laser Acq.
Threshold	0.5 mm
#Completeness	99.6%
Mean	1.9 μm
RMS Error	73 μm

Table 4 Reconstruction performance of the SW for STC Images.

Table 4 reports the results of the comparison. As far as the accuracy of the reconstruction is concerned, the obtained RMS values are all well below the instrument scientific requirements at the breadboard scale (with a pixel scale of 105 μm).
Considering the scale factor between the SVS and the nominal operative configuration of STC the vertical precision obtained corresponds to 36 m (taking into account an on ground pixel of 58 metres at first orbit around Mercury).

5.4. STEREO_ANGLE test

The STEREO ANGLE test intends to focus on the dependence of the reconstruction performance on the local slope of the surface. Three synthetic stereo couples are generated using the method described in 5.1. The reference DTM is the DTEEC_002661_1895_003294_1895_U01.IMG produced using ISIS and SOCET Set (copyright BAE Systems) software as described in Kirk et al. (2008). The DTM has a pixel scale of 1.0 m and has been generated with the HiRISE stereo pair PSP_002661_1895 and PSP_003294_1895.
The DTM is imported with its orthophoto in Blender and the simulated stereo images are generated through raytracing technique fixing three stereo blocks with the same on ground pixel (4.6 m on image plane) and stereo angles respectively of ±10°, ±15°, ±20°.
The stereo images are shown in ***Figure 8***. In the figure we also present the an enlarged regions of the anaglyphs to make evident the increasing of the parallax map with the stereo angle.

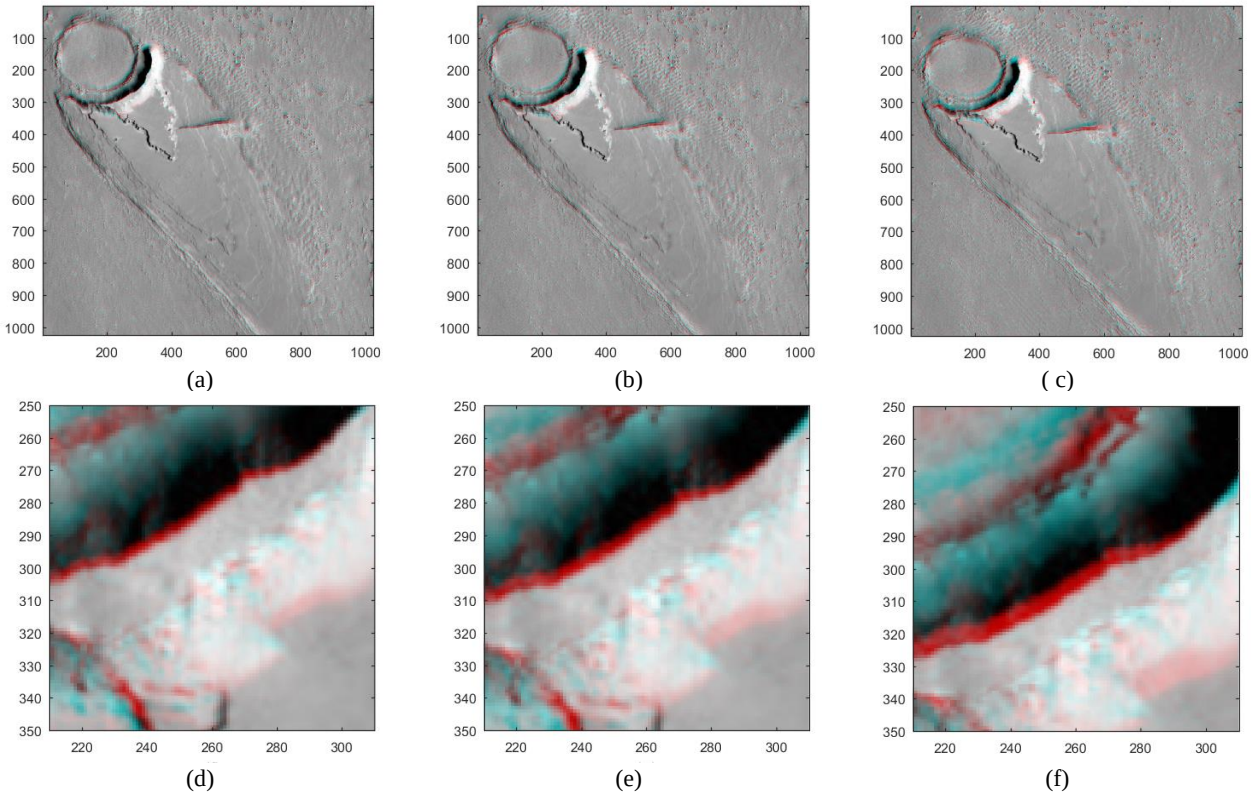

Figure 8 *Images show the anaglyphs of the stereo couple generated synthetically. In (a,b,c) the stereo couples respectively of ±10, ±15, ±20°. In (d,e,f) the same region of the three stereo couple is shown enlarged for better understanding.*

The same pipeline is run on the three stereo couples. The generated DTMs are then compared with the reference DTMs.
The resulting error maps are shown in ***Figure 9*** together with the local slope of the reference DTM. The error strongly increases with the increase of the stereo angle.
The sub-pixel final refinement of the 3DPD pipeline is based on the use of affine transformations that produce larger errors for the steeper slopes. The greatest errors are concentrated for all the three cases around the region with the steepest slope. Improvement will be obtained by applying more complex shape functions for geometric modelling of the parallax distortion in the LSM implementation [45].
The increase of the stereo angle enlarges the regions with large error which appear more extended in the DTM with $\pm 20°$ than in the DTM with $\pm 10°$.

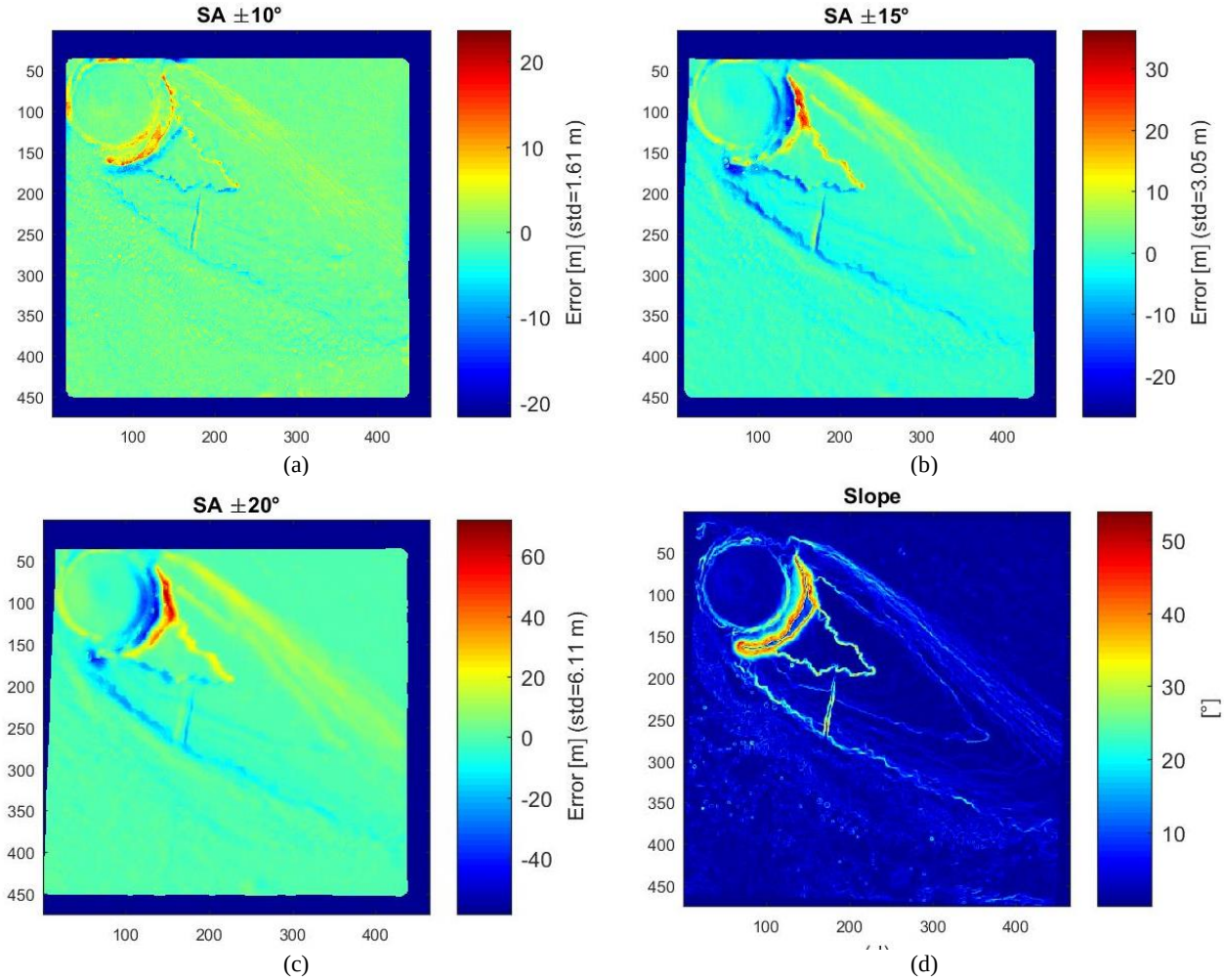

Figure 9 *Figures (a), (b),(c) show the Error maps of DTMs generated by the synthetical images respectively with a Stereo Angle (SA) of ±10, ±15, ±20°. In (d) the local slope of the reference DTMs is shown.*

The reconstruction error and so the local reliability of the DTM produced are functions of the local slope and this effect increases with the stereo angle adopted. For higher stereo angle the affine transformation is not enough to model the panoramic/perspective effect. The expected vertical precision (EP)[46] in three cases (considering a matching error of 1 pixel) is reported in **Table 5** together with the RMSE of the discrepancies obtained. For a better understanding of the EP definition see Appendix 6.

For the tests performed the matching error reaches values lower than 1/10 of the pixel for the first case and increases for higher stereo angles.

Figure 10a shows the distribution of the absolute value of the reconstruction error on z-axis in the three stereo block acquisition cases evaluated. In (b) these errors are correlated with local slope. The curves represent the local median of the absolute errors for different values of slopes.

The local slope has strong an impact on the prospective effect of the two images which is defined even by the stereo angle. Local slope and stereo angles degrades the reconstruction precision as shown in **Table 5**. For low slopes (<5°) the pipeline guarantees a vertical precision between 0.4 and 0.86 m in the three cases. For high slopes (>35°) the median error increases to 5.2m in the case of low stereo angles and reaches 16m for the higher ones.

Data	Unit	SA ±*10°*	SA ±*15°*	SA ±*20°*
Reference			HiRiSe DTM	
Vertical Precision [1px]	[m]	12.6	8.5	6.4
RMS Error [m]	[m]	1.61	3.05	6.11
Median absolute error (low slope)	[m]	0.4	0.6	0.86
Median absolute error (high slope)	[m]	5.2	9.6	16
Slope Degradation	[%/°]	2.9	8.7	15.65

Table 5 *Reconstruction performance of the 3DPD for SLOPE-TEST images*

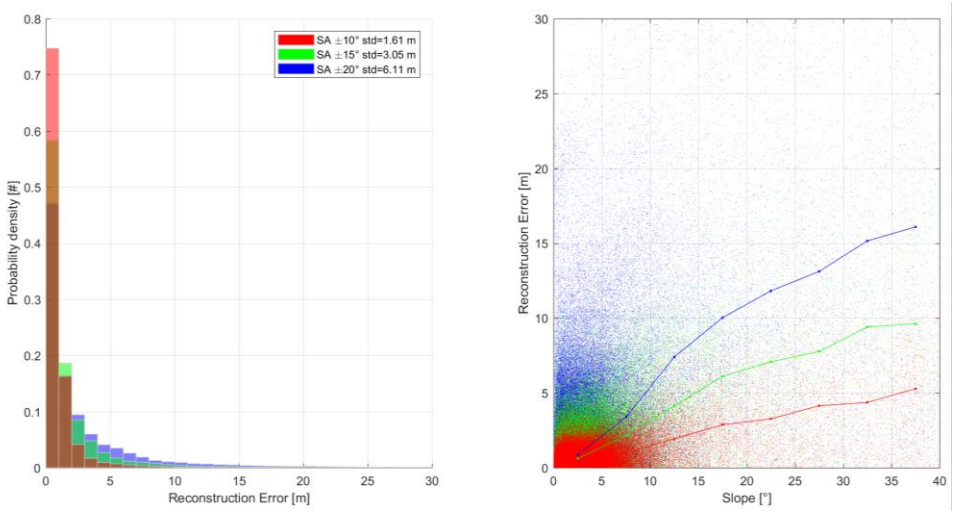

(a) (b)

Figure 10 *In (a) the distribution of the reconstruction error in metres for the three cases analysed. In (b) the error as function of the local slope.*

In the three cases of emission considered the degradation of the VP due to the slopes becomes stronger with higher emission angles. The red curve for instance (emission angle of 10°) increases by 2.9% with each degree of slope while the blue one (emission angle of 20°) increases by more than 15%/degree showing the lower tolerance of the pipeline to higher slopes.

CONCLUSIONS

A photogrammetric stereo processing workflow has been developed for the 3D reconstruction from CaSSIS images. The pipeline includes a procedure for the image pre-processing management and different approaches for the stereo image matching. Two different tests based on synthetic and real images are presented to validate the pipeline. At the same time, the first stereo images acquired by the CaSSIS instrument have been processed to achieve the best possible accuracy relying on a preliminary distortion map and the exploitation of the first version of the Spice Kernels data.
The tests have demonstrated the capabilities of the SW to provide a three-dimensional product from the CaSSIS stereo images. It implements several methods and tools that are now used routinely for the generation of the DTMs from stereo images acquired from the nominal orbit of the primary science phase.

The software will be a starting point for the future procedures that will be also applied to Stereo Camera (STC) images for the BepiColombo mission to Mercury. The multiple tools integrated in the software package are able to generate cartographic products, including Digital Terrain Models (DTMs), ortho images and other auxiliary stereo products. These data are suitable for science analysis as well as public outreach.
Among the activities concerning the 3DPD, it has been decided that all the DTMs generated by the institutes involved in the CaSSIS team will be collected in Padova where the repository [4] will be hosted and made accessible to the public via a dedicated web page.

Acknowledgements

This activity has been realized under the Italian Space Agency ASI-INAF agreement no.2017-03-17. The authors wish to thank the spacecraft and instrument engineering teams for the successful completion of the instrument. CaSSIS is a project of the University of Bern and funded through the Swiss Space Office via ESA's PRODEX programme. The instrument hardware development was also supported by the Italian Space Agency (ASI) (ASI-INAF agreement no.I/018/12/0), INAF/Astronomical Observatory of Padova, and the Space Research Center (CBK) in Warsaw. Support from SGF (Budapest), the University of Arizona (Lunar and Planetary Lab.) and NASA are also gratefully acknowledged. Stepan Tulyakov was supported through NCCR PlanetS. A special acknowledgement to Gianfranco Forlani and Riccardo Roncella, of the DICATeA of the University of Parma, for the support on using the Dense Matcher software, that has been important in the definition of the 3DPD architecture.

6. APPENDIX: Vertical Precision Assumptions

The EP (often defined only for nadiral cameras) depends preliminary on three factors:

-The camera used to acquire the image (depending by sensor pixel dimension p and focal length c)
-The geometry used for the stereo acquisition (depending by baseline B and height H of the acquisition block)
-The performance of the algorithm applied for determination of the parallax.

If the first two factors are defined by the geometry and the instrument, the third parameter is not easily defined a priori and it needs a deep investigation supported by a testing set-up.
The maximum relative vertical accuracy as scales following the equation:

$$\boldsymbol{v_{EP}^{rel}} = \sqrt{2}\, \boldsymbol{r_c}\, \boldsymbol{r_s}\, \boldsymbol{r_\alpha}\, \boldsymbol{\sigma_{pxy}} \tag{4}$$

Where: $\boldsymbol{\sigma_{pxy}}$ is the parallax error, r_c is the camera component, r_s the stereo geometry component. The out-nadir correction r_α (a factor negligible in the case nadir parallel block acquisition) is here introduced in the well-known equation this case, where the not nadiral configuration introduce an angle α (emission angle) between nadiral direction and one of the line of sight.
A synthetic scheme of the definition of these parameters is shown in **Error! Reference source not found.**.

	Dependence	**Definition**
Camera	ξ angle subtended by a pixel,	$r_c = \tan(\xi)$
Baseline geometry	ω the angle defining stereo block geometry.	$r_s = \tan(\omega)$
Not-Nadiral Correction	β the semi-FoV of the camera and α emission angle	$r_\alpha = \frac{cos^2(\beta)}{\cos^2(\alpha+\beta)}$
Parallax error	Algorithm, surface morphology and reflection characteristic, perspective	$\boldsymbol{\sigma_{pxy}}$

Table 6 Main components of the vertical error in the reconstruction. Their definition is well shown in **Error! Reference source not found.**.

Substantially the vertical relative accuracy can be described by 4 different angles. This means that it is not dependent by linear transformation on the geometry of the acquisition block and can be scaled as an acquisition system.
Differently by classical nadiral configuration maximal error is achieved at the boundary of the FoV (which justify the presence of the β angle in the definition of out-nadir correction) and the factor $\sqrt{2}$ is introduced to include the propagation of the parallax error deriving by the matching error on epipolar lines and the orthogonal ones (associated to geometrical estimation of the acquisition block).
If all the other parameters can be easily evaluated (a description of their context is shown in **Error! Reference source not found.**), parallax error $\boldsymbol{\sigma_{pxy}}$ (expressed normally in pixels) depends by the performance of the algorithm and the photogrammetric pipeline applied, by the texture of the target, the variegation of the surface, the illumination condition [35], the local contrast and the quality of the images [33],the perspective introduced by the stereo block and the quality of the images.

All this task effects can be studied separately but a calibration validation represents a needed investigation for the empirical estimation of this term and the influence of all these issues on it.

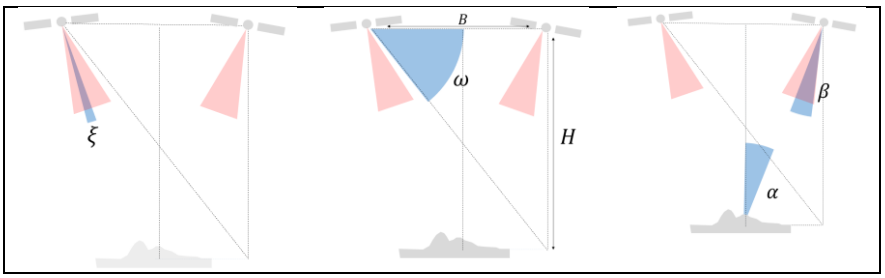

(a) (b) (c)

Figure 11 *Definition of the component of the maximal stereo relative error. All images show the not nadiral configurations defined by a height H and a baseline B with an emission angle of α. Red angles represent the FoV of the instrument. In (a) the angle ξ, the camera component describing the intrinsic parameters. In (b) the angle ω representing the block acquisition geometry and in (c) the so called Not-Nadiral correction defined by the on-ground angle α and the half field of view β . Out-nadir correction can be considered equal to one in nadir approximation.*

Without considering the FoV and the not nadiral configuration ($\alpha, \beta = 0$) the equation 4) can be reduced by more known following equation:

$$v_{EP} = \frac{p_{og} H}{B}$$

Where p_{og} is the pixel on ground.
The v_{EP} decreases with the stereo angle because it does not depend by the matching error and it is just matter of the better precision of the triangulation.
On the other side the RSM increases with the stereo angle because of the rise of the perspective and of the matching error.
The ratio of these two values, the RSM and the vertical precision, represents the matching error.

If all the v_{EP} can be easily evaluated and the RMS value can be measured, the matching error will depend by:

- the performance of the algorithm and the photogrammetric pipeline applied,
-by the texture of the target, the variegation of the surface,
-the illumination condition[46],
-the local contrast and the quality of the images,
-the perspective introduced by the stereo block and the quality of the images.

References:

[1] Cremonese, Gabriele, et al. "The stereo camera on the BepiColombo ESA/JAXA mission: a novel approach." *Advances in Geosciences* 15 (2009): 305 10.1142/9789812836229_0019

[2] Thomas, N., Cremonese, G., Banaszkiewicz, M., Bridges, J., Byrne, S., Da Deppo, V., ... & Ivanov, A. (2014, July). The colour and stereo surface imaging system (CaSSIS) for ESA's Trace Gas Orbiter. In Abstract 1067 presented at the 8th International Conference on Mars.10.1007/s11214-017-0421-1

[3] Cremonese, G., & Re Re, C. (2018, September). The CaSSIS Digital Terrain Model generation and Archiving at OAPD. In European Planetary Science Congress (Vol. 12). 10.5194/isprs-archives-XLII-3-W1-133-2017

[4] https://cassis.oapd.inaf.it/archive/

[5] Ziyuan, O., Chunlai, L., Yongliao, Z., Hongbo, Z., Chang, L., Jianzhong, L., ... & Wei, B. (2010). Chang'E-1 lunar mission: An overview and primary science results. 空间科学学报, 30(5), 392-403. 10.1007/s11430-010-4056-2h

[6] R. Jaumann et al., The high-resolution stereo camera (HRSC) experiment on Mars Express: Instrument aspects and experiment conduct from interplanetary cruise through the nominal mission. Planetary and Space Science 55 (2007) 928–952 10.1016/j.pss.2006.12.003

[7] Ohtake, Makiko, et al. "Performance and scientific objectives of the SELENE (KAGUYA) Multiband Imager." Earth, planets and space 60.4 (2008): 257-264 10.1186/BF03352789

[8] Robinson, M. S., et al. Lunar reconnaissance orbiter camera (LROC) instrument overview. Space Science Reviews 150.1 (2010): 81-124.10.1007/s11214-010-9634-2

[9] Bell III, J. F., et al. "Calibration and performance of the Mars reconnaissance orbiter context camera (CTX)." International Journal of Mars Science and Exploration 8 (2013): 1-14 10.1555/mars.2013.001

[10] Simioni, E., et al. " SIMBIOSYS-STC ready for launch: a technical recap" International Conference on Space Optics—*ICSO 2018, 1118042 (12 July 2019);* 10.1117/12.2536065

[11] Da Deppo, V., Naletto, G., Cremonese, G., & Calamai, L. (2010). Optical design of the single-detector planetary stereo camera for the BepiColombo European Space Agency mission to Mercury. Applied optics, 49(15), 2910-2919. 10.1364/AO.49.002910

[12] McEwen, Alfred S., et al. "Mars reconnaissance orbiter's high resolution imaging science experiment (HiRISE)." Journal of Geophysical Research: Planets 112.E5 (2007). 10.1029/2005JE002605

[13] Keller, Horst Uwe, et al. "OSIRIS–The scientific camera system onboard Rosetta." Space Science Reviews 128.1-4 (2007): 433-506. 10.1007/s11214-006-9128-4

[14] Polyansky, I., et al. "Stereo topographic mapping concept for the upcoming Luna-Resurs-1 orbiter mission." Planetary and Space Science (2017). 10.1016/j.pss.2017.09.013

[15] Chew, L. P. (1989). Constrained delaunay triangulations. Algorithmica, 4(1-4), 97-108. 10.1007/BF01553881

[16] Ching, Wee-Soon. "Normalized cross-correlation: the contrast-dependent problem and its solution." Journal of Electronic Imaging 4.3 (1995): 278-283. 10.1109/ROBOT.2006.1641826

[17] Acton, C.H.; "Ancillary Data Services of NASA's Navigation and Ancillary Information Facility;" Planetary and Space Science, Vol. 44, No. 1, pp. 65-70, 1996. 10.1016/0032-0633(95)00107-7

[18] BAY, Herbert, et al. Speeded-up robust features (SURF). Computer vision and image understanding, 2008, 110.3: 346-359. https://doi.org/10.1016/j.cviu.2007.09.014

[19] Simioni, E., Re, C., Mudric, T., Pommerol, A., & Thomas, N. (2017). A Photogrammetric Pipeline for the 3D Reconstruction of CaSSIS images on board ExoMars TGO. The International Archives of Photogrammetry, Remote Sensing and Spatial Information Sciences, 42, 133-139.10.5194/isprs-archives-XLII-3-W1-133-2017

[20] Gruen, Armin. Adaptive least squares correlation: a powerful image matching technique. South African Journal of Photogrammetry, Remote Sensing and Cartography 14.3 (1985): 175-187.

[21] Baker, Simon, and Iain Matthews. Lucas-kanade 20 years on: A unifying framework. International journal of computer vision 56.3 (2004): 221-255 10.1023/B:VISI.0000011205.11775.fd

[22] Simioni, E., Naletto, G., Forlani, G., Cremonese, G., Da Deppo, V., Massironi, M., & Segato, E. (2011). A new stereo algorithm based on snakes. Photogrammetric Engineering & Remote Sensing, 77(5), 495-507. 10.14358/PERS.77.5.495

[23] Kent, B. R. (2014). 3D scientific visualization with blender. Morgan & Claypool Publishers.10.1088/978-1-6270-5612-0

[24] Szeliski, Richard. "Image alignment and stitching: A tutorial." Foundations and Trends® in Computer Graphics and Vision 2.1 (2006): 1-104. *10.1561/0600000009*

[25] *Lewis, John P. "Fast template matching." Vision interface. Vol. 95. No. 120123. 1995*

[26] Becerra, P., Sori, M. M., Thomas, N., Pommerol, A., Simioni, E., Sutton, S. S., ... & Cremonese, G. (2019). Timescales of the climate record in the south polar ice cap of Mars. Geophysical Research Letters. 10.1029/2019GL083588

[27] Briechle, Kai, and Uwe D. Hanebeck. "Template matching using fast normalized cross correlation." Optical Pattern Recognition XII. Vol. 4387. International Society for Optics and Photonics, 2001. 10.1117/12.421129

[28] Stein, A., Huertas, A., Matthies, L. (2006). Attenuating stereo pixel-locking via affine window adaptation. IEEE International Conference on Robotics and Automation, pp. 914–921

[29] *Mi*ller, S. B., and A. S. Walker, Die Entwicklung der digitalen photogrammetrischen Systeme von Leica und Helava, Z. Photogramm. Fernerkundung,1(95), 4 –16, 1995 10.1029/2007JE003000

[30] Stein, A. N., Huertas, A., & Matthies, L. (2006, May). Attenuating stereo pixel-locking via affine window adaptation. In Proceedings 2006 IEEE International Conference on Robotics and Automation, 2006. ICRA 2006. (pp. 914-921). IEEE.

[31] Gruen, Armin. Adaptive least squares correlation: a powerful image matching technique. South African Journal of Photogrammetry, Remote Sensing and Cartography 14.3 (1985): 175-187.

[32] Cremonese, G., Simioni, E., Re, C., Mudric, T., Lucchetti, A., Massironi, M., ... & Thomas, N. (2017, March). First Mars surface stereo reconstruction with the CaSSIS stereo camera. In Lunar and Planetary Science Conference (Vol. 48). 2017LPI....48.1464C

[33] Massironi, M., Pozzobon, R., Lucchetti, A., Simioni, E., Re, C., Mudric, T., ... & Thomas, N. (2017). A three dimensional geological reconstruction of Noctis Labyrinthus slope tectonics from CaSSIS data. EPSC abstract. 2017EPSC...11..618M

[34] https://cassis.oapd.inaf.it/archive/

[35] Gruen, Armin. "Development and status of image matching in photogrammetry." The Photogrammetric Record 27.137 (2012): 36-57. 10.1111/j.1477-9730.2011.00671.x

[36] Roloff, V., et al. "On-ground performance and calibration of the ExoMars trace gas orbiter CaSSIS imager." Space science reviews 212.3-4 (2017): 1871-1896. 10.1007/s11214-017-0404-2

[37] Quantin, C., et al. "Oxia Planum, the landing site for ExoMars 2018." 47th Lunar and Planetary Science Conference Abstracts, Abstract. Vol. 2863. 2016. EPSC2015/EPSC2015-704

[38] Tulyakov S., Running NASA Ames Pipeline with TGO CaSSIS, https://github.com/tlkvstepan/CaSSIS_stereo, Accessed: 01 April 2019.

[39] Smith, David E., et al. "The lunar orbiter laser altimeter investigation on the lunar reconnaissance orbiter mission." Space science reviews 150.1-4 (2010): 209-241. 10.1029/2001GL013832

[40] Re, C., Tulyakov, S., Simioni, E., Mudric, T., Cremonese, G., and Thomas, N.: Performance evaluation of 3dpd, the photogrammetric pipeline for the cassis stereo images, Int. Arch. Photogramm. Remote Sens. Spatial Inf. Sci., XLII-2/W13, 1443-1449, https://doi.org/10.5194/isprs-archives-XLII-2-W13-1443-2019, 2019. 10.5194/isprs-archives-XLII-2-W13-1443-2019

[41] Da Deppo, V., Naletto, G., Cremonese, G., Debei, S., & Flamini, E. (2006, June). A novel optical design for planetary surface stereo-imaging: preliminary design of the Stereoscopic Imaging Channel of SIMBIOSYS for the BepiColombo ESA mission. In Space Telescopes and Instrumentation I: Optical, Infrared, and Millimeter (Vol. 6265, p. 626527). International Society for Optics and Photonics. 10.1117/12.670286

[42] Simioni, E., Da Deppo, V., Naletto, G., Cremonese, G., & Re, C. (2014, May). Stereo Camera for satellite application: A new testing method. In 2014 IEEE Metrology for Aerospace (MetroAeroSpace) (pp. 582-587). IEEE. 10.1109/MetroAeroSpace.2014.6865992

[43] Re, C., et al. "Effects of image compression and illumination on digital terrain models for the stereo camera of the BepiColombo mission." *Planetary and Space Science* 136 (2017): 1-14. 10.1016/j.pss.2016.10.018

[44] Kirk, R. et al. (2003), High- resolution topomapping of candidate MER landing sites with Mars Orbiter Camera narrowangle images, J. Geophys. Res., 108(E12), 8088, doi:10.1029/2003JE002131.

[45] Re, C., Roncella, R., Forlani, G., Cremonese, G., & Naletto, G. (2014). Evaluation of an area-based matching algorithm with advanced shape models. ISPRS Annals of Photogrammetry, Remote Sensing & Spatial Information Sciences, 2(4). 10.5194/isprsannals-I-4-209-2012

[46] R.L.Kirk. The effect of illumination on stereo dtm quality:simulations in support of europa exploration. ISPRS Annals of the Photogrammetry, Remote Sensing and Spatial Information Sciences, Volume III-4, 2016 XXIII ISPRS Congress, 12–19 July 2016, Prague, Czech Republic 10.5194/isprs-annals-III-4-103-2016